Japanese Journal of Applied Physics

STAP ARTICLE

Spectroscopic ellipsometry studies on β-Ga_2O_3 films and single crystal

Japanese Journal of Applied Physics **55**, 1202B2 (2016)
http://doi.org/10.7567/JJAP.55.1202B2

Spectroscopic ellipsometry studies on β-Ga_2O_3 films and single crystal

Takeyoshi Onuma[1,2*], Shingo Saito[2], Kohei Sasaki[3,2], Tatekazu Masui[3], Tomohiro Yamaguchi[1], Tohru Honda[1], Akito Kuramata[3], and Masataka Higashiwaki[2]

[1]*Department of Applied Physics, Kogakuin University, Hachioji, Tokyo 192-0015, Japan*
[2]*National Institute of Information and Communications Technology, Koganei, Tokyo 184-8795, Japan*
[3]*Tamura Corporation, Sayama, Saitama 350-1328, Japan*

*E-mail: onuma@cc.kogakuin.ac.jp

Received April 27, 2016; accepted July 22, 2016; published online September 21, 2016

Anisotropic optical properties are investigated on β-Ga_2O_3 films and a single crystal by spectroscopic ellipsometry measurements. The $(\bar{2}01)$ films grown on (0001) α-Al_2O_3 contain threefold in-plane rotational domains, and the refractive index and absorption coefficient α obtained by assuming an isotropic material are found to be smaller than those in the single crystal. By measuring the off-normal transmission ellipsometry spectra of the (010) β-Ga_2O_3 substrate, the optical anisotropy in a biaxial crystal as well as the gradual increase in α are recognized as origins of the scattering in optically determined bandgap energies.

1. Introduction

Monoclinic β-Ga_2O_3 is an emerging material because of its potential applications in UV transparent electrodes,[1] photodetectors,[2,3] field-effect transistors (FETs),[4] and Schottky barrier diodes.[5,6] The availability of large-area single-crystalline substrates[7] grown by melt-growth methods, such as the floating zone (FZ) and edge-defined film-fed growth methods, epitaxial growth technique,[8–10] selective doping by the ion implantation technique,[11] etc. offer greater flexibility for designing β-Ga_2O_3-based high-power and high-voltage FETs. After the first demonstration of metal-semiconductor FETs,[4] the achievement was followed by the demonstration of depletion-mode metal–oxide–semiconductor FETs.[12] The device characteristics are further improved by optimizing the device structure[13] as well as by obtaining high-structural-quality homoepitaxial layers.[10]

Despite its superior material properties, there are a number of issues that should be solved when measuring the fundamental optical properties. As shown in Figs. 1(b) and 1(c), β-Ga_2O_3 has a base-centered monoclinic structure with a space group symmetry of C^3_{2h} $(C2/m)$.[14] Since the first experimental observation of its bandgap energy (E_g) of 4.59 eV at 300 K,[15] E_g at room temperature (RT) scattered between 4.4 and 5.0 eV.[8,15–17] The ambiguity may be induced by the low crystal symmetry, where valence bands construct 18 bands and transitions from half of them to the conduction band minimum (CBM) at the Γ point are dipole-allowed. Valence band ordering has been investigated in our previous study by polarized transmittance and reflectance sectroscopies.[18] The energies of the absorption edge (E_{edge}) have been determined as 4.48, 4.57, and 4.70 eV for the electric field vector of incidence light parallel to the c-, a^*-, and b-axes, respectively. Here, the a^*-axis is perpendicular to the (100) plane and is angled at $-13.7°$ from the a-axis. The study has also pointed out that the absorption coefficient α for the direct transition from the upper most valence band to the CBM at Γ was found to be small ($10^2 \leq \alpha \leq 10^3\,cm^{-1}$), and the values gradually increased with increasing transition energy ($\alpha > 10^5\,cm^{-1}$ for $E > 5\,eV$). These characteristic optical anisotropies were found to be causes of scattering in the reported E_g values.[8,15–17] In this study, anisotropic optical properties are further investigated on β-Ga_2O_3 films and a single crystal by spectroscopic ellipsometry (SE) measurements.[19]

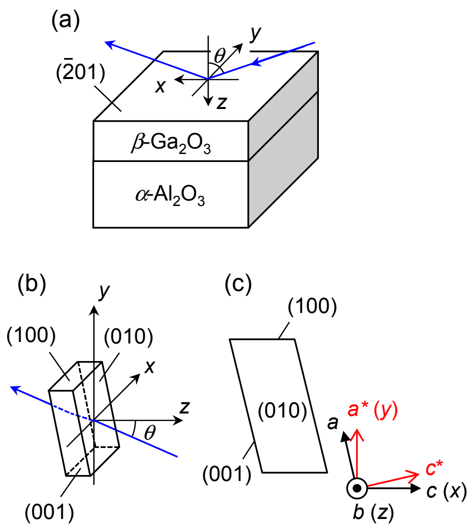

Fig. 1. (Color online) (a) Configurations of observed x-, y-, and z-axes for (a) reflection and (b) transmission SE measurements. (c) Projection of the unit cell along the surface normal b-axis of the (010) plane of β-Ga_2O_3. θ is the incidence angle.

2. Experimental procedure

As shown in Fig. 1(a), 150–700-nm-thick $(\bar{2}01)$ unintentionally doped β-Ga_2O_3 films were grown on (0001) α-Al_2O_3 substrates at 850 °C for 1 h by molecular beam epitaxy. Ga was supplied by a Knudsen cell and the oxygen source was supplied by an ozone (5%)–oxygen (95%) gas mixture. X-ray diffraction measurements exhibited full widths at half maximum of $(\bar{4}02)$ diffraction peak of $\Delta 2\theta = 0.93$–$1.1°$ for θ–2θ patterns and $\Delta\omega = 1.5$–$2.3°$ for rocking curves. The SE measurements of the films were conducted using a J. A. Woolam M2000 system at RT for wavelengths from 193 to 1700 nm. As shown in Figs. 1(b) and 1(c), a (010) Mg-doped semi-insulating β-Ga_2O_3 substrate was prepared by the FZ growth method.[7] Off-normal transmission ellipsometry spectra were measured using a J. A. Woolam RC2 system. The plane of incidence contains both the incidence light vector and the surface normal. The observed x- and y-axes are defined as being parallel and perpendicular to the plane of incidence, and the axes are perpendicular to the surface normal z-axis. The incidence angle θ is defined as the angle

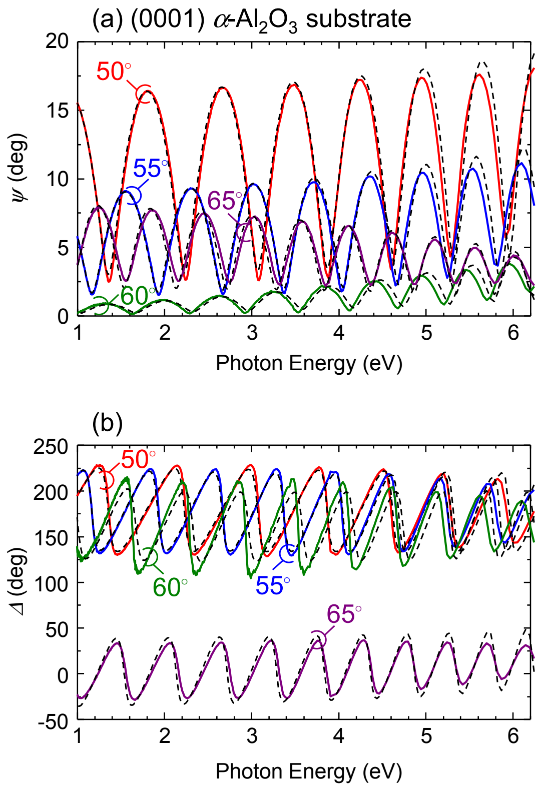

Fig. 2. (Color online) SE data (solid lines) and fittings (broken lines) of (0001) α-Al_2O_3 substrate. (a) and (b) show Ψ and Δ spectra, respectively.

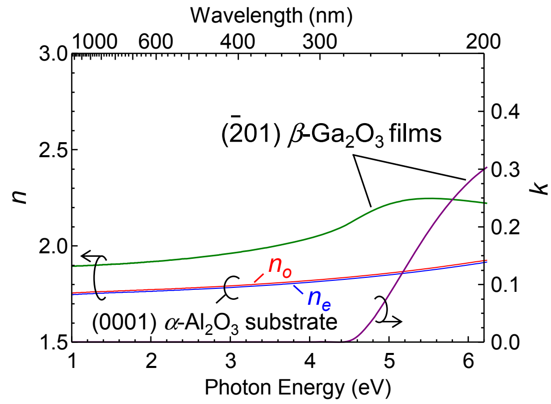

Fig. 3. (Color online) Spectra for refractive index n and extinction coefficient k of $(\bar{2}01)$ β-Ga_2O_3 films grown on the (0001) α-Al_2O_3 substrates. Spectra for the n values of the ordinary (n_o) and extraordinary (n_e) rays in the (0001) α-Al_2O_3 substrate are also shown.

from the surface normal, and it was set at 50, 55, 60, and 65° for the β-Ga_2O_3 films and 50, 60, and 70° for the substrate. The ellipsometers measure Ψ and Δ given by

$$\frac{r_{pp}}{r_{ss}} = \tan\Psi \exp(i\Delta), \tag{1}$$

$$\frac{t_{pp}}{t_{ss}} = \tan\Psi \exp(i\Delta), \tag{2}$$

where r_{pp}, r_{ss}, t_{pp}, and t_{ss} are the Fresnel reflection and transmission coefficients for the p- and s-polarized lights, respectively.[19)]

3. Results and discussion

The SE data and fittings of the bare (0001) α-Al_2O_3 substrate are shown in Fig. 2. α-Al_2O_3 has a rhombohedral structure. It is a uniaxial crystal, whose optic axis is parallel to the c-axis. In general, off-diagonal elements in the dielectric tensor,

$$\boldsymbol{\varepsilon} = \begin{pmatrix} \varepsilon_{xx} & \varepsilon_{xy} & \varepsilon_{xz} \\ \varepsilon_{yx} & \varepsilon_{yy} & \varepsilon_{yz} \\ \varepsilon_{zx} & \varepsilon_{zy} & \varepsilon_{zz} \end{pmatrix}, \tag{3}$$

induce the cross coupling of the p- and s-polarized lights.[19,20)] In particular, the dielectric tensor of the crystals in which three crystallographic axes have an orthogonal coordinate, such as cubic, tetragonal, hexagonal, rhombohedral, and orthorhombic systems, can be diagonalized by rotating the crystallographic orthogonal coordinate with the Euler angles so as to coincide with the observed xyz-axes.[19,20)] In the measurements, the optic c-axis was set to be parallel to the observed z-axis, enabling us to independently determine optical constants for the ordinary and extraordinary rays without using the generalized-SE or Mueller matrix ellipsometry.[21–23)] Multiple data sets were analyzed using the Cauchy function in the transparent spectral range. The optical anisotropy was evaluated using the uniaxial layer mode in WVASE32,[24)] where the spectral dispersion of the refractive index for the ordinary ray n_o along the x-axis was first determined, and that for the extraordinary ray n_e along the z-axis was given by their difference $\Delta n = n_o - n_e$. Regression analysis using the Levenberg–Marquardt algorithm[25)] gave mean squared error (MSE) as low as 13 with a surface roughness of 1.9 nm. As shown in Fig. 3, Δn is small in a range of 0.007–0.010, which is in good agreement with the previous report.[26)] By using the optical constants as substrate values, the SE data of the $(\bar{2}01)$ β-Ga_2O_3 films grown on the (0001) α-Al_2O_3 substrates were analyzed, as shown in Fig. 4. β-Ga_2O_3 is known as a biaxial crystal, whose optic axis is parallel to the b-axis. The nonvanishing off-diagonal elements in the dielectric tensor induce the cross coupling of the p- and s-polarized lights. However, the β-Ga_2O_3 films heteroepitaxially grown on (0001) α-Al_2O_3 generally contain threefold in-plane rotational domains,[8)] intuitively triggering us to assume the films as an isotropic material. Optical anisotropy will be rigorously discussed later in the β-Ga_2O_3 substrate. Multiple-data-sets for the 157- and 695-nm-thick films were first analyzed using the Cauchy function in the transparent spectral range. Then, to determine the optical constants in the absorbing spectral range, a point-to-point fit was carried out using the B-Spline approach in WVASE32,[24)] where the refractive index n and extinction coefficient k were evaluated so as to maintain the Kramers–Kronig relationship. The numerically derived data were then analytically fitted using the model dielectric function including the Tauc–Lorentz and UV pole functions. Regression analysis gave an MSE of 13 with a surface roughness of 3.3–8.8 nm, ensuring the quality of the fitting and giving reliable sets of optical constants, as shown in Fig. 3. The obtained n values reasonably agree well with the previously reported data for the polycrystalline films,[27)] and E_g is determined to be 4.4 eV.

Transmission SE data and fittings of the (010) β-Ga_2O_3 substrate are shown in Fig. 5. As already mentioned, β-Ga_2O_3 is a biaxial crystal, whose optic axis is parallel to the b-axis. In particular, the angle $\beta = 103.7°$ between the a- and c-axes[14)] leaves the off-diagonal element nonvanishing as

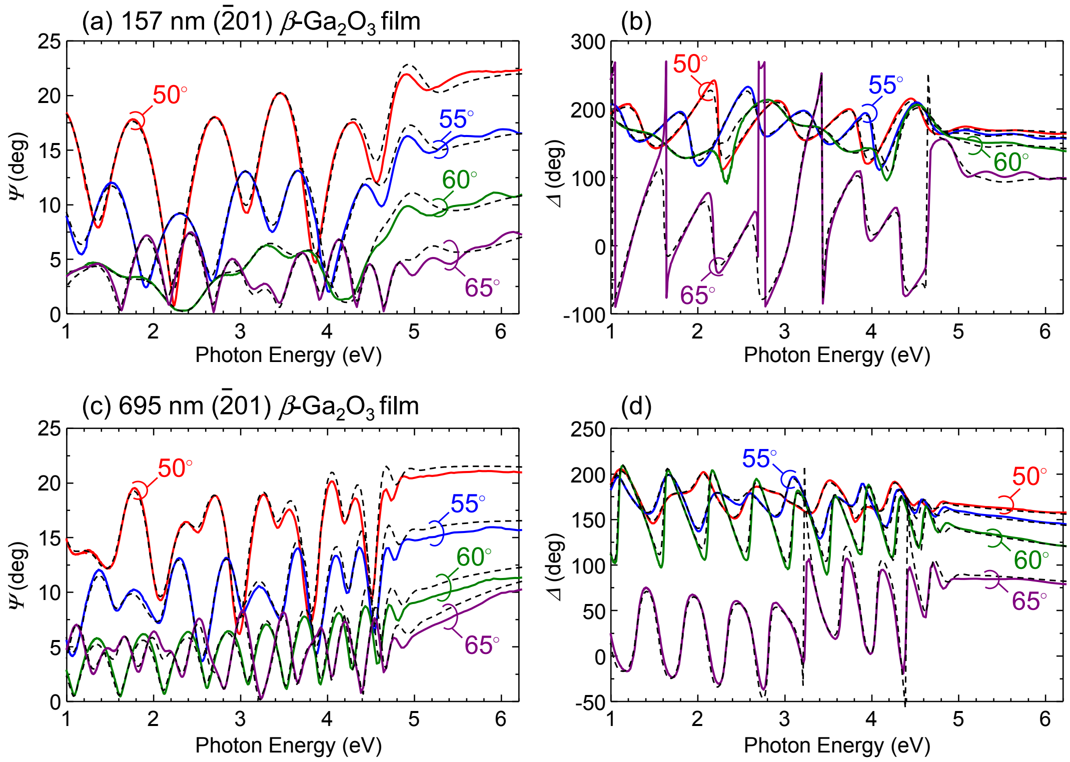

Fig. 4. (Color online) SE data (solid lines) and fittings (broken lines) of ($\bar{2}01$) β-Ga_2O_3 films grown on the (0001) α-Al_2O_3 substrates. (a) and (b) show Ψ and Δ spectra for the 157-nm-thick film, respectively, and (c) and (d) show corresponding data sets for the 695-nm-thick film.

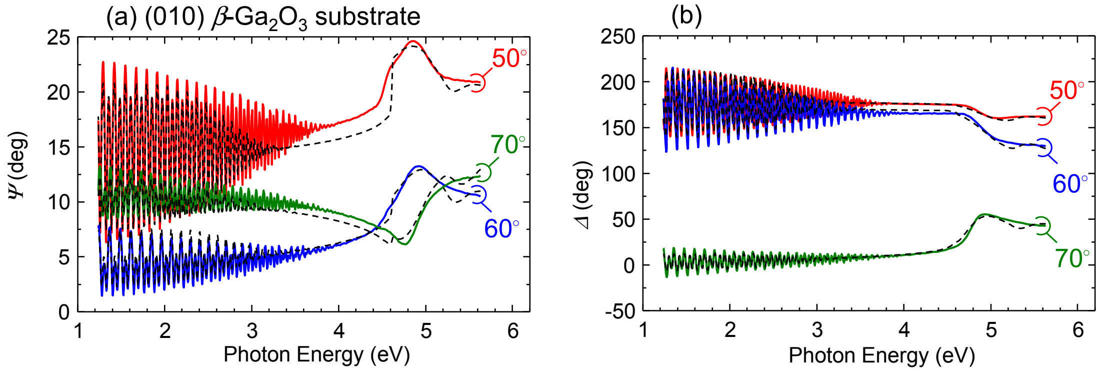

Fig. 5. (Color online) Transmission SE data (solid lines) and fittings (broken lines) of (010) β-Ga_2O_3 substrate. (a) and (b) show Ψ and Δ spectra, respectively.

$$\boldsymbol{\varepsilon} = \begin{pmatrix} \varepsilon_{xx} & \varepsilon_{xy} & \\ \varepsilon_{xy} & \varepsilon_{yy} & \\ & & \varepsilon_{zz} \end{pmatrix}. \tag{4}$$

The off-diagonal element ε_{xy} induces the cross coupling of the p- and s-polarized lights through the color-dependent rotation of the dielectric ellipsoid in the *ac*-plane around the *b*-axis.[20] Moreover, the real and imaginary parts of the dielectric function have different rotation angles.[20,28,29] According to the Mueller matrix ellipsometry study on single crystals,[30] ε_{xy} is small ($|\varepsilon_{xy}| < 0.02$) in the transparent spectral range, but it reaches values up to 0.30 in the absorbing spectral range and the cross coupling of the polarized lights cannot be neglected. In this study, the optical anisotropy was evaluated using the biaxial layer mode in WVASE32,[24] where the spectral dispersion of the optical constant along the *z*-axis (*b*-axis) is first determined, and those along the *x*-axis (*c*-axis) and *y*-axis (a^*-axis) are given by the differences. Indeed, the data reflect the dielectric constants that projected the dielectric ellipsoid on the observed *x*-, *y*-, and *z*-axes. Although the information acquired is less than that obtained by Mueller matrix ellipsometry[21–23,30] where the projected components and ε_{xy} are simultaneously determined, the present measurements still give reasonable sets of optical constants.

The multiple data sets were first analyzed using the Cauchy function in the transparent spectral range. Then, to determine the optical constants in the absorbing spectral range, a point-to-point fit was carried out using the B-Spline approach.[24] The numerically derived data were then analytically fitted using the model dielectric function including the Tauc–Lorentz and UV and IR pole functions. Regression analysis gave a relatively large MSE of 25 with a surface roughness of 3.6 nm, by reflecting the weak absorption at around 300 nm presumably due to defects and/or impurities. Spectra for the

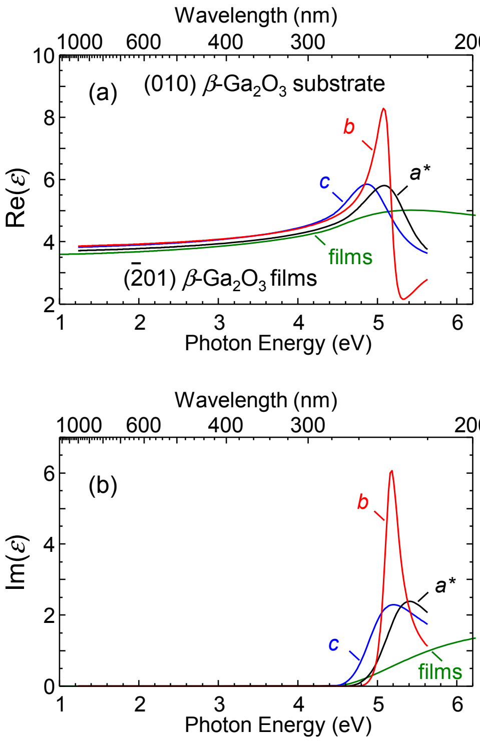

Fig. 6. (Color online) Spectra for (a) real [Re(ε)] and (b) imaginary [Im(ε)] parts of the dielectric function of ($\bar{2}$01) films and (010) substrate.

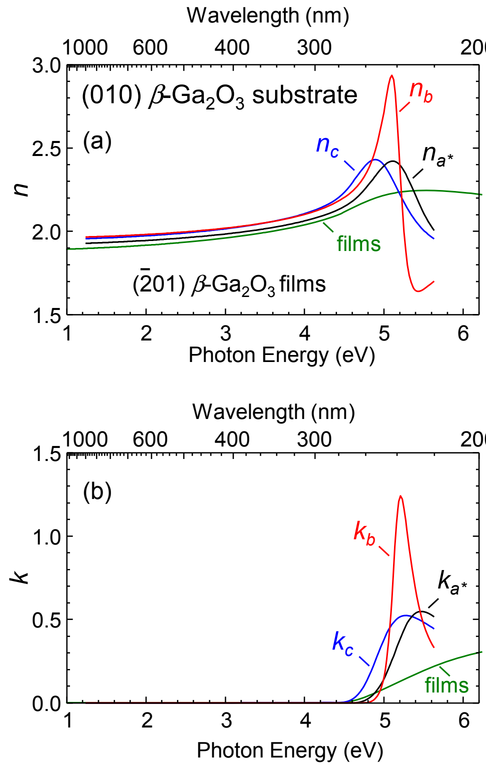

Fig. 7. (Color online) Spectra for (a) refractive index n and (b) extinction coefficient k of ($\bar{2}$01) films and (010) substrate.

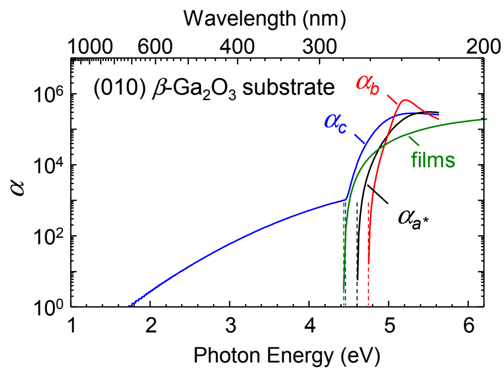

Fig. 8. (Color online) Spectra for absorption coefficient α of ($\bar{2}$01) films and (010) substrate. E_g values are indicated by the vertical broken lines.

real [Re(ε)] and imaginary [Im(ε)] parts of the dielectric function are shown in Fig. 6. The data for the ($\bar{2}$01) β-Ga_2O_3 films are also shown for comparison. As shown in Fig. 7(a), the refractive indexes have values along the a^*- (n_{a^*}), c- (n_c), and b- (n_b) axes in order of energy in the transparent spectral range, and the order is changed in the absorbing spectral range. The onset energies of the k values show the same order as the previously determined[18] E_{edge} values along the c- (k_c), a^*- (k_{a^*}), and b- (k_b) axes owing to the interband transitions from the upper most valence bands to the CBM. The absorption coefficients α along the c- (α_c), a^*- (α_{a^*}), and b- (α_b) axes are shown in Fig. 8. The values for the ($\bar{2}$01) β-Ga_2O_3 films are also shown for comparison. Here, the weak absorption at around 300 nm in the substrate is reflected in the spectrum along the c-axis. The values of n and α obtained for the films are found to be smaller than those in the single crystal presumably owing to the crystallinity. As shown by the vertical broken lines, E_g was estimated to be 4.458, 4.605, and 4.744 eV along the c-, a^*-, and b-axes, respectively, which are in good agreement with the previously reported E_{edge} values.[18] The results also show the same trends in terms of α as discussed previously,[18] i.e., α for the transition from the upper most valence band at Γ to the CBM is small on the order of 10^3 cm^{-1}, and it gradually increases up to 10^6 cm^{-1} at around 5.2 eV. The characteristic optical anisotropy as well as the gradual increase in α are eventually recognized as origins of the scattering in the reported E_g values.[8,15–17]

4. Conclusions

Anisotropic optical properties were investigated on β-Ga_2O_3 films and a single crystal by SE measurements. Since the ($\bar{2}$01) films heteroepitaxially grown on (0001) α-Al_2O_3 substrates contain threefold in-plane rotational domains, SE data were analyzed by assuming an isotropic material. The obtained n values reasonably agreed well with the previously reported data for polycrystalline films.[27] To rigorously discuss the optical anisotropy in a biaxial crystal, off-normal transmission ellipsometry spectra were measured for the (010) β-Ga_2O_3 substrate. The optical constants determined along the crystallographic c-, a^*-, and b-axes reasonably agreed with our previous data,[18] which were measured by polarized transmittance and reflectance spectroscopies. The values of n and α obtained for the films were found to be smaller than those in the single crystal presumably owing to the crystallinity. The characteristic optical anisotropy as well as the gradual increase in α were further recognized as origins of the scattering in the reported E_g values.[8,15–17]

Acknowledgments

The authors would like to thank Dr. T. Sato of J. A. Woollam Japan Co., Inc. for technical support on the SE measurements. This work was supported in part by Grants-in-Aid for Scientific Research Nos. 25390071, 25289093, 25420341, and 25706020 from MEXT, Japan.

1) N. Ueda, H. Hosono, R. Waseda, and H. Kawazoe, Appl. Phys. Lett. **70**, 3561 (1997).
2) Y. Kokubun, K. Miura, F. Endo, and S. Nakagomi, Appl. Phys. Lett. **90**, 031912 (2007).
3) T. Oshima, T. Okuno, N. Arai, N. Suzuki, S. Ohira, and S. Fujita, Appl. Phys. Express **1**, 011202 (2008).
4) M. Higashiwaki, K. Sasaki, A. Kuramata, T. Masui, and S. Yamakoshi, Appl. Phys. Lett. **100**, 013504 (2012).
5) T. Oishi, Y. Koga, K. Harada, and M. Kasu, Appl. Phys. Express **8**, 031101 (2015).
6) M. Higashiwaki, K. Konishi, K. Sasaki, K. Goto, K. Nomura, Q.-T. Thieu, R. Togashi, H. Murakami, Y. Kumagai, B. Monemar, A. Koukitu, A. Kuramata, and S. Yamakoshi, Appl. Phys. Lett. **108**, 133503 (2016).
7) Details of the substrate preparation are available at http://www.tamura-ss.co.jp/en/gao/.
8) T. Oshima, T. Okuno, and S. Fujita, Jpn. J. Appl. Phys. **46**, 7217 (2007).
9) K. Sasaki, A. Kuramata, T. Masui, E. G. Víllora, K. Shimamura, and S. Yamakoshi, Appl. Phys. Express **5**, 035502 (2012).
10) H. Murakami, K. Nomura, K. Goto, K. Sasaki, K. Kawara, Q.-T. Thieu, R. Togashi, Y. Kumagai, M. Higashiwaki, A. Kuramata, S. Yamakoshi, B. Monemar, and A. Koukitu, Appl. Phys. Express **8**, 015503 (2015).
11) K. Sasaki, M. Higashiwaki, A. Kuramata, T. Masui, and S. Yamakoshi, Appl. Phys. Express **6**, 086502 (2013).
12) M. Higashiwaki, K. Sasaki, T. Kamimura, M. H. Wong, D. Krishnamurthy, A. Kuramata, T. Masui, and S. Yamakoshi, Appl. Phys. Lett. **103**, 123511 (2013).
13) M. H. Wong, K. Sasaki, A. Kuramata, S. Yamakoshi, and M. Higashiwaki, 1st Int. Workshop Gallium Oxide and Related Materials, 2015, J1.
14) S. Geller, J. Chem. Phys. **33**, 676 (1960).
15) H. H. Tippins, Phys. Rev. **140**, A316 (1965).
16) N. Ueda, H. Hosono, R. Waseda, and H. Kawazoe, Appl. Phys. Lett. **71**, 933 (1997).
17) T. Matsumoto, M. Aoki, A. Kinoshita, and T. Aono, Jpn. J. Appl. Phys. **13**, 1578 (1974).
18) T. Onuma, S. Saito, K. Sasaki, T. Masui, T. Yamaguchi, T. Honda, and M. Higashiwaki, Jpn. J. Appl. Phys. **54**, 112601 (2015), and references cited therein.
19) H. Fujiwara, *Spectroscopic Ellipsometry* (Maruzen, Tokyo, 2011) 2nd ed.
20) M. Born and E. Wolf, *Principles of Optics: Electromagnetic Theory of Propagation, Interference and Diffraction of Light* (Cambridge University Press, Cambridge, U.K., 1999) 7th expanded ed.
21) M. Schubert, Phys. Rev. B **53**, 4265 (1996).
22) M. Schubert, *Infrared Ellipsometry on Semiconductor Layer Structures* (Springer, Heidelberg, 2004).
23) M. Schubert, R. Korlacki, S. Knight, T. Hofmann, S. Schöche, V. Darakchieva, E. Janzén, B. Monemar, D. Gogova, Q.-T. Thieu, R. Togashi, H. Murakami, Y. Kumagai, K. Goto, A. Kuramata, S. Yamakoshi, and M. Higashiwaki, Phys. Rev. B **93**, 125209 (2016).
24) J. A. Woollam Co., Inc., Guide to Using WVASE32.
25) G. E. Jellison, Jr., Thin Solid Films **313–314**, 33 (1998).
26) H. Yao and C. H. Yan, J. Appl. Phys. **85**, 6717 (1999).
27) M. Rebien, W. Henrion, M. Hong, J. P. Mannaerts, and M. Fleischer, Appl. Phys. Lett. **81**, 250 (2002).
28) M. Dressel, B. Gompf, D. Faltermeier, A. K. Tripathi, J. Pflaum, and M. Schubert, Opt. Express **16**, 19770 (2008).
29) G. E. Jellison, Jr., M. A. McGuire, L. A. Boatner, J. D. Budai, E. D. Specht, and D. J. Singh, Phys. Rev. B **84**, 195439 (2011).
30) C. Sturm, J. Furthmüller, F. Bechstedt, R. Schmidt-Grund, and M. Grundmann, APL Mater. **3**, 106106 (2015).